Environ Sci Pollut Res (2013) 20:6638–6645
DOI 10.1007/s11356-013-1694-x

RESEARCH ARTICLE

Hydrothermal synthesis of meso/macroporous $BiVO_4$ hierarchical particles and their photocatalytic degradation properties under visible light irradiation

Puttaswamy Madhusudan · Malahalli Vijaya Kumar · Tadashi Ishigaki · Kenji Toda · Kazuyoshi Uematsu · Mineo Sato

Received: 6 December 2012 / Accepted: 28 March 2013 / Published online: 26 April 2013

Abstract An ordered hierarchical meso/macroporous monoclinic bismuth vanadate ($BiVO_4$) particle was fabricated for the first time by a simple two-step melamine template hydrothermal method followed by calcination. The physiochemical parameters of as-prepared porous materials were characterized by means of X-ray diffraction, scanning electron microscopy, high-resolution transmission electron microscopy, Raman, Barrett–Emmett–Teller, and UV–vis techniques. The nitrogen adsorption–desorption measurement and pore size distribution curve suggest that meso/macropores exist in these hierarchical microarchitectures. Further, it is found that melamine plays a significant role in the formation of porous $BiVO_4$ particles, and when a known amount of melamine was added, the surface area and pore size of such porous $BiVO_4$ particles were increased. The photocatalytic activities of the as-prepared hierarchical $BiVO_4$ samples were measured for the photodegradation of Congo red aqueous dye solution under visible light irradiation. Surprisingly, the porous $BiVO_4$ particles showed outstanding photocatalytic activities than polycrystalline $BiVO_4$ sample. The possible enhancement of such catalytic performance has also been further discussed.

Keywords Meso/macropore $BiVO_4$ · Photocatalysis · Visible light · Photodegradation · Melamine · Congo red

Responsible editor: Philippe Garrigues

P. Madhusudan (✉)
Department of Earth Science, University of Mysore,
Mysore 570006, India
e-mail: madhujpn@gmail.com

M. V. Kumar
Department of Interdisciplinary Space Sciences, Japan Aerospace Exploration Agency (JAXA), Tsukuba, Ibaraki 305-8505, Japan

T. Ishigaki · K. Uematsu
Centre for Trandisciplinary Research, Niigata University,
8050 Ikarashi 2-nocho,
Niigata 950-2181, Japan

K. Toda
Graduate School of Science and Technology, Niigata University,
8050 Ikarashi 2-nocho,
Niigata 950-2181, Japan

Present Address:
P. Madhusudan · M. Sato
Department of Chemistry and Chemical Engineering,
Niigata University, 8050 Ikarashi 2-nocho,
Niigata 950-2181, Japan

Introduction

In the past three decades, a lot of investigations have been focused on the fabrication of various non-titania-based visible light semiconductor photocatalyst for their wide applications in degradation of organic compounds. Among the various non-titania-based visible light driven semiconductor photocatalyst, vanadates like bismuth vanadate ($BiVO_4$) (Tokunaga et al. 2001; Kudo et al. 2004; Li et al. 2008), $InVO_4$ (Ye et al. 2002; Zhang et al. 2006a), YVO_4 (Xu et al. 2007), and $CeVO_4$ (Mahapatra et al. 2007; Mahapatra et al. 2008) have attracted most scientific attention for their high photocatalytic activities. Contrarily, $BiVO_4$ as an important fundamental material has received great interest because of its potential applications in various fields, such as photocatalytic degradation of organic pollutants (Zhang et al. 2007), air purification and water splitting (Kato et al. 2004), ferroelasticity (Hazen and Mariathasan 1982; Lim et al. 1995; Lim et al. 1992), ionic conductivity (Hirota et al.

1992), and organic dye (Galembeck and Alves 2002; Zhang et al. 2006b). Furthermore, $BiVO_4$ exists in three different phases, monoclinic sheelite, tetragonal zircon, and tetragonal sheelite structure (Kudo et al. 1998, 1999). The photocatalytic properties of $BiVO_4$ are strongly related to its crystal phase; for example, the photocatalytic activity of monoclinic phase is much higher than that of other two (Kohtani et al. 2003). $BiVO_4$ with monoclinic structure shows relatively narrow band gap energy (2.4 eV) compared to that of $BiVO_4$ with tetragonal phase (3.1 eV). Over the past few years, synthesis of monoclinic $BiVO_4$ has been accomplished by several methods such as metalorganic decomposition (Galembeck and Alves 2000), hydrothermal treatment (Liu et al. 2003; Yu and Kudo 2006; Ke et al. 2009; Sun et al. 2009), coprecipitation (Ke et al. 2008; Chen et al. 2008), solid state reaction (Sleight et al. 1979; Gotić et al. 2005), and sonochemical technique (Zhou et al. 2007). Nonetheless, most of these synthetic strategies have only brought further $BiVO_4$ materials with large crystal sizes and low surface area. Thus, it serves a serious problem for their photocatalytic applications because a high surface area is required to speed up the adsorption/desorption kinetics of organic pollutants on the surface of $BiVO_4$ (Zhou et al. 2010a). In addition, the activity of pure $BiVO_4$ still needs to be improved due to its poor adsorptive performance and difficult migration of photogenerated electron–hole pairs (Gotić et al. 2005).

Recently, a great progress has been developed to fabricate porous materials, by using surfactants or soft templates (Zhang and Zhang 2009; Ren et al. 2009; Shang et al. 2009; Yin et al. 2010; Xu et al. 2011). However, all these strategies to improve the surface area of $BiVO_4$ materials are less favorable from the technological point of view, as they may add impurities and increase the overall cost of production, thus rendering large-scale technical production difficulties. As a result, it is of great importance to develop new synthesis strategy to fabricate meso/macroporous monoclinic $BiVO_4$ photocatalysts with high surface area to improve the photocatalytic activity. To the best of our knowledge, the preparation and photocatalytic activity of meso/macroporous $BiVO_4$ has not yet been systematically reported.

Herein, for the first time, meso/macroporous $BiVO_4$ photocatalyst was prepared by using an amorphous $BiVO_4$ gel as a precursor under hydrothermal method. It is found that the addition of melamine as a template in starting $BiVO_4$ gel materials played a vital role in controlling the size of porous $BiVO_4$ particles. Further, the as-prepared monoclinic porous $BiVO_4$ hierarchical particles demonstrate an outstanding spectral selectivity compared with polycrystalline $BiVO_4$ and showed higher photocatalytic activities for degradation of Congo red (CR) aqueous dye solution under visible light irradiation.

Experimental

Photocatalyst preparation

The preparation procedure of meso/macroporous $BiVO_4$ particles consists of two steps. Firstly, vanadium stock solution was prepared by stirring stoichiometric amount of NH_4VO_3 (Kanto Chemical Co., Inc, Japan) in distilled water for 20 min. Then, a known amount of $Bi(NO_3)_3{\cdot}5H_2O$ (Wako Pure Chemical Industries) was dissolved in 4 M HNO_3 aqueous solution. Further, as-prepared both stock solutions were mixed together, respectively, according to Bi/V molar ratio of 1 to obtain a greenish yellow suspension. Then, $NH_3{\cdot}H_2O$ solution was added dropwise until the pH reached 7. The suspension was aged for 24 h and resultant precipitates were filtered, washed five times with ethanol and distilled water, respectively, and dried in a vacuum oven at 80 °C for 8 h. In a second step, the as-prepared 1 g of $BiVO_4$ precursor gel was mixed with 5 g of melamine (Kanto Chemical Co., Inc, Japan) and hydrothermally treated at 180 °C for 2 h. The system was allowed to cool to room temperature and the corresponding final products were dried at 60 °C in air for 2 h. Furthermore, the as-prepared powders were calcined in a muffle furnace at 600 °C for 2 h in air to increase $BiVO_4$ porous structure and crystallinity. For comparison, we also prepared polycrystalline $BiVO_4$ powders without melamine addition keeping other experimental conditions constant.

Characterization

The powder X-ray diffraction (XRD) patterns of the as-prepared samples were obtained on an X-ray diffractometer (MX-Labo; Mac Science Ltd.,) using monochromatic Cu Kα (0.15418 nm) at 0.02° scan speed. The accelerating voltage and the applied current were 40 kV and 25 mA, respectively. Scanning electron microscopy (SEM) images were recorded by (JEOL JSM-5310MVB, Japan) at an accelerating voltage of 10 kV. Transmission electron microscopy (TEM) and high-resolution transmission electron microscopy (HRTEM) analyses were conducted using JEM-1200EX electron microscopy (JEOL, Japan) operating at 120 kV. The nitrogen absorption–desorption isotherm was obtained at 77 K by a nitrogen adsorption apparatus (Autosorb-1MP; Quantachrome Instruments, Boynton Beach) utilizing Barrett–Emmett–Teller (BET) calculation of specific surface area and nonlocal density functional theory calculation of pore volume and pore size (diameter) distributions. Raman spectra were recorded at room temperature using a micro-Raman spectrometer (Renishaw InVia) in the back-scattering geometry with a 514.5-nm Ar^+ laser as an excitation source. UV–vis absorbance spectra were obtained for the dry-pressed disk samples with a UV–vis

spectrophotometer (Jasco, V-550, Japan). Fine $BaSO_4$ powder was used as a standard.

Evaluation of photocatalytic activity

Photocatalytic activities of $BiVO_4$ samples were evaluated by the photocatalytic degradation of CR under visible light using 300 W Xe lamp with a 420-nm cutoff filter as a light source. A beaker of 100 mL was used as a reaction vessel, and the distance between the lamp and the solution was 20 cm. The experiments were performed at room temperature as follows: 0.1 g of photocatalyst was dispersed into 20 mL of CR aqueous solution (1×10^{-5} mol L^{-1}). Prior to irradiation, the suspensions were magnetically stirred in dark for 10 h to ensure the adsorption/desorption equilibrium between the photocatalyst powder and the solution. At an interval of 15 min, 5 mL of suspensions was centrifuged to remove the photocatalyst powders and 3 mL of CR aqueous solution was used for analyses. After each analysis, the extracted CR aqueous solution was restored into the beaker. Evaluation of the photocatalytic activities of the photocatalyst was conducted by recording the variations of the absorption band maximum through a UV–vis spectrophotometer (Hitachi U-3010). CR dye concentration was analyzed by recording the variations in the absorption band maximum at 497 nm. The decolorization pseudo-first-order reaction and its kinetics may be expressed as $\ln(C_0/C)=kt$, where k is the apparent reaction rate constant, C_0 is the initial absorbance of aqueous CR dye solution, t is the reaction time, and C is the absorbance of aqueous CR at t, while k is determined by a linear regression method.

Results and discussion

Phase structure and morphology

The influence of the melamine addition on the formation of $BiVO_4$ crystalline phase has been investigated by XRD. The XRD patterns of the $BiVO_4$ samples prepared at different conditions are shown in (Fig. 1). After annealing at 600 °C for 2 h, the as-prepared products exhibited sharp peaks indicating high degree of crystallinity. All the diffraction patterns are well indexed as pure monoclinic $BiVO_4$ (JCPDS 14-0688 with a=5.195 Å, b=11.701 Å, and c=5.092 Å), indicating the introduction of melamine did not change the lattice structure of $BiVO_4$. Furthermore, the diffraction intensity of porous $BiVO_4$ sample increased with respect to polycrystalline $BiVO_4$ sample and no diffraction peaks assigned to melamine were observed, which also suggest that $BiVO_4$ is single phase. Furthermore, it was expected that as-synthesized porous $BiVO_4$ particles would have high photocatalytic efficiency due to their distinct monoclinic phase structure and high intensity.

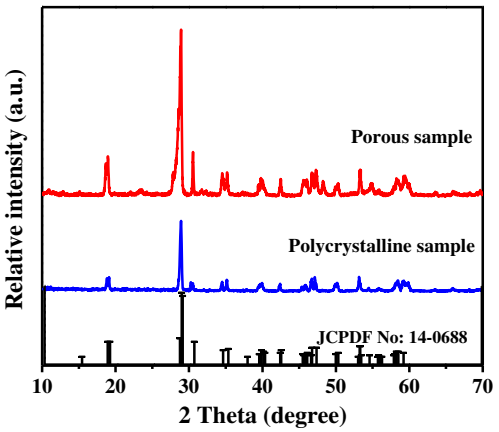

Fig. 1 XRD patterns of meso/macroporous and polycrystalline $BiVO_4$ particles obtained in the presence of melamine along with the standard XRD pattern of monoclinic $BiVO_4$

The representative microstructure of polycrystalline and porous $BiVO_4$ particles are shown in Fig. 2. The image in Fig. 2a demonstrates that the polycrystalline $BiVO_4$ particles obtained without melamine is well crystallized with large particles of 800–900 nm in size. Generally, photocatalytic activity decreases as particle size increases because the number of active photocatalytic sites decreases with an increasing size. Figure 2b, c shows typical SEM image of hierarchical meso/macroporous $BiVO_4$ structures, which are composed of several pores with an average of 400–600 nm in diameter. According to the above observations, the as-prepared porous $BiVO_4$ sample consists of several meso/macropore channels interconnected with bigger particles. Also, it is well known that the thermal decomposition of melamine leads to the formation of condensation products like melam, melem and melon, and ammonia gas. Further, the incorporation of melamine in our experimental system resulted in the liberation of vapors and gases, which probably might have played an important role for the formation of $BiVO_4$ porous microstructures. Further, the well-developed porous structure and morphology of $BiVO_4$ sample were also confirmed by a high-magnification TEM and HRTEM image. Figure 3a shows typical TEM image of spherical meso/macroporous $BiVO_4$ particles with an average crystallite size of 500–600 nm. The crystallite size estimated based on TEM micrographs matches well with the size calculated by SEM observation. Figure 3b shows a typical HRTEM image of porous $BiVO_4$ particle recorded on the edge of the nanoparticles. The clear lattice fringe indicates the high-crystallinity and single-crystalline nature of the porous $BiVO_4$ nanoparticles. The fringe spacing of 0.255 nm agrees with the spacing of the (020) lattice plane of monoclinic $BiVO_4$. It has also been reported that small grain size and high crystallinity provide higher photocatalytic activity for the increased reactive sites and promote

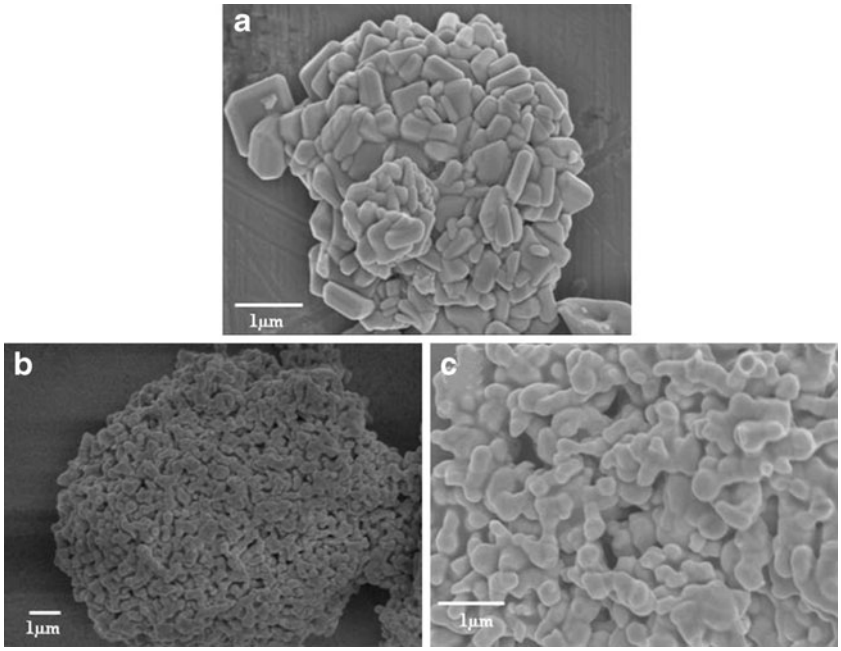

Fig. 2 **a**–**c** SEM images of polycrystalline and meso/macroporous $BiVO_4$ particles

electron–hole separation efficiency (Amano et al. 2008). Thus, as-prepared meso/macroporous particles were expected to show enhanced photocatalytic performance.

Raman spectra of $BiVO_4$ samples

Raman spectroscopy is helpful in examining the local structure of the synthesized $BiVO_4$ meso/macroporous particles. The Raman spectra were recorded from wave number in the range of 200–1,000 cm^{-1}. Figure 4 shows the Raman spectra of as-prepared samples. The Raman spectra obtained on hydrothermally prepared meso/macroporous $BiVO_4$ particles show the same features as previously reported on polycrystalline $BiVO_4$ powders prepared by metalorganic decomposition method (Galembeck and Alves 2000). All four characteristic Raman bands at 330, 375, and 821 cm^{-1} of monoclinic sheelite structure are well documented (Li et al. 2008; Madhusudan et al. 2011). A strong band at around 821 cm^{-1} is attributed to the symmetrical V–O stretching mode and a weak shoulder at about 716 cm^{-1} can be assigned to antisymmetric V–O stretching mode (Zhang et al. 2008). The bands at ca. 330 and 373 cm^{-1} are attributed to symmetric V–O (A_g) bending mode and antisymmetric V–O (B_g) bending mode of VO_4, respectively. The signal at 373 cm^{-1} is stronger than that of 330 cm^{-1} because of the symmetric defaults in VO_4 tetrahedral. The peak position at 205 cm^{-1} can be attributed to the external modes (rotational/translation) (Zhou et al. 2010b). Further, the intensity of the peaks increases with the addition of melamine. This can be attributed to the formation of larger number of meso/macroporous and broader range of size distribution.

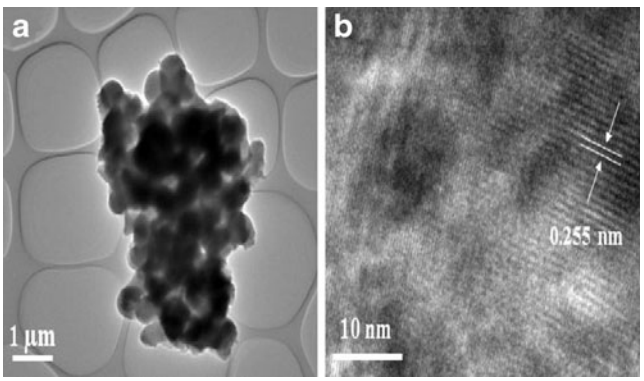

Fig. 3 **a**, **b** TEM and HRTEM image of meso/macroporous $BiVO_4$ particles showing the lattice fringes

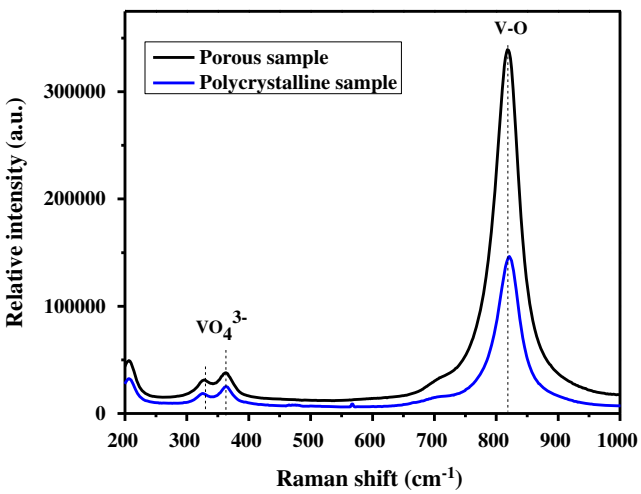

Fig. 4 Raman spectra of meso/macroporous and polycrystalline $BiVO_4$ particles

BET surface area and pore size distributions

The nitrogen adsorption–desorption isotherms of as-prepared samples are shown in Fig. 5. The polycrystalline $BiVO_4$ sample displays type III (Brunauer–Beming–Deming–Teller classification) isotherm, which characteristically indicates that weak interaction between N_2 molecules and the samples. In contrast, porous $BiVO_4$ sample shows type IV isotherms with very narrow hysteresis loops at relative pressures between 0.2 and 1.0, indicating the pore size distribution in the mesoporous and macroporous region (Sing et al. 1985). At lower relative pressure, the shape of the hysteresis loop is of type H2, suggesting the existing of ink bottle-type pores. While at high relative pressure range, the hysteresis loops is of type H3, indicating the presence of slit-shaped pores (Jiang et al. 2009; Xu et al. 2008). Moreover, the adsorption branch of nitrogen isotherms shows a steady increase at P/P_0 approaching unity, possibly due to the presence of macropores (>50 nm). In fact, the mesopores and macropores are formed within the $BiVO_4$ and large inter-aggregated pores formed between $BiVO_4$ particles. The pore size distribution (inset in Fig. 5) is broad in the range from 3 to over 60 nm. It shows mesopores with pore diameter about 3.4 nm and macropores at about 48.5 nm, which are associated with the smaller voids within $BiVO_4$ particles and the textural larger pores that are formed between particles, further confirming the existence of mesopores and macropores. These results demonstrate the formation of hierarchically nanoporous structures in porous $BiVO_4$ sample on a multilength scale. In general, the porous structures are extremely useful in photocatalysis because they assure an efficient transport of reactant and product molecules, in addition to facilitating the absorption of pollutants for degradation. Table 1 shows BET surface area, pore volume, and average pore size of as-prepared samples.

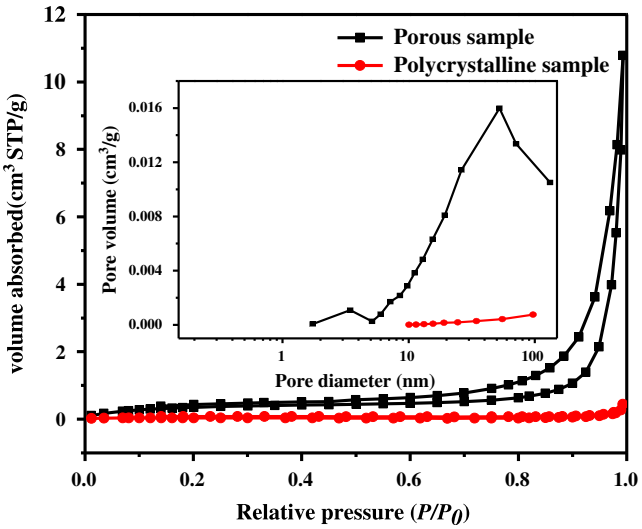

Fig. 5 Nitrogen adsorption–desorption isotherms and the corresponding pore–size distribution curves (*inset*) of as-prepared samples

Photophysical properties

It is well known that the optical absorption of a semiconductor is closely related to its electronic structure. The UV–vis diffuse reflectance spectra of polycrystalline and porous $BiVO_4$ samples are shown in Fig. 6. Significant differences in the absorption edge between the polycrystalline $BiVO_4$ and porous $BiVO_4$ sample were observed. All samples shows strong absorption in the UV–vis region from 200 to 550 nm. A steep absorption edge at 519 nm of polycrystalline $BiVO_4$ sample spectrum indicates that the visible light absorption is due to the intrinsic band gap transition. It is presumed that melamine decomposition at high temperature leads to the formation of loose and porous $BiVO_4$ particles. Interestingly, as can be seen, the absorption edges of porous $BiVO_4$ sample are red shifted with comparison to that of polycrystalline sample suggesting a decrease in crystal size. Furthermore, the enhanced optical absorption property of porous $BiVO_4$ results mainly from the multiple reflection of incident light in the mesoporous particles. The absorption edge of a spectrum reflects the energy difference between the top of the valence band and the bottom of the conduction band. That is to say, the band gap of the semiconductor can be calculated from the absorption edge. Further, the Kubelka–Munk function based was employed to determine the band gap. For the indirect band gap semiconductor, the relation between the absorption coefficient (α) and photo energy ($h\nu$) can be written as:

$$\alpha = B_{\mathrm{ind}}(h\nu - \mathrm{Eg})^2/h\nu \quad (1)$$

where B_{ind} is absorption constant for indirect transitions. α can be determined from the scattered and reflectance spectra according to Kubelka–Munk theory (Patterson et al. 1977). The indirect band baps estimated from the Kubelka–Munk

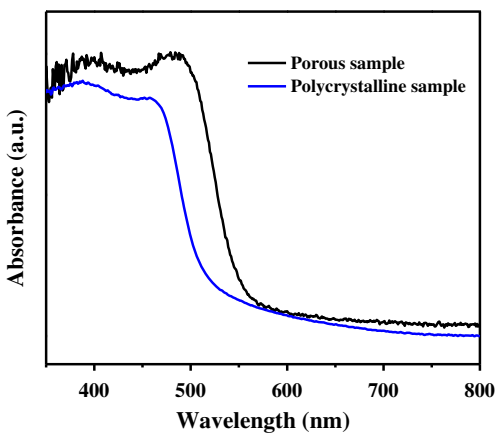

Fig. 6 UV–vis absorption spectra of as-prepared samples

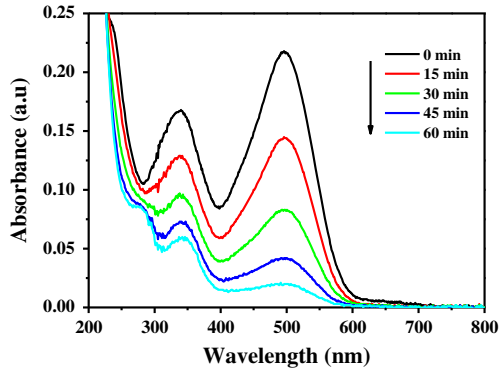

Fig. 7 Absorption changes of CR aqueous solution in the presence of meso/macroporous $BiVO_4$ particles under visible light irradiation

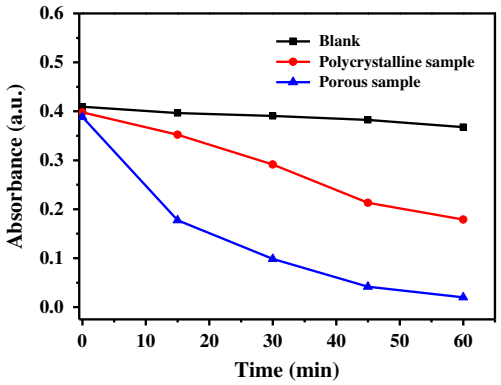

Fig. 9 Amount of absorbance of CR aqueous solution as a function of time in the presence of as-prepared samples

function are ca. 2.34 and 2.13 eV for polycrystalline and porous $BiVO_4$ samples, respectively, which are consistent with previous results (Tokunaga et al. 2001; Zhang and Zhang 2009; Stoltzfus et al. 2007). Compared with polycrystalline $BiVO_4$ particles, the band gap of porous $BiVO_4$ particles slightly decreased, presumably due to particle size resulting from porous structures. This indicates that the meso/macroporous $BiVO_4$ particles have a suitable band gap for photocatalytic decomposition of organic contaminants under visible light irradiation.

Photocatalytic properties

Because of the unique structure and high BET-specific surface area, the meso/macroporous $BiVO_4$ particles may possess high adsorption capacity towards degradation of pollutants in water. Thus, the photocatalytic performance of as-prepared samples for the removal of CR aqueous dye solution with a major absorption band at 497 and 347 nm was chosen as a model organic compound. Figure 7 shows the temporal change of absorption spectra of dye solutions exposed to visible light as a function of time in the presence of porous $BiVO_4$ sample. As shown with the increasing photodegradation time, the absorption peak intensity of CR solution drops gradually and almost disappears after 60 min, exhibiting excellent photocatalytic activity in the degradation of CR over the as-prepared sample. Figure 8 shows the comparison of photocatalytic activities of as-prepared samples. It is demonstrated that the self-degradation of CR is extremely slow; only 3 % of CR is photolyzed after 60 min irradiation. In contrast, when $BiVO_4$ samples as photocatalysts were added in the CR solution, the degradation efficiency of CR significantly increases and no new peaks in the UV or visible region could be noticed. The results suggest that, in the presence of polycrystalline $BiVO_4$ or porous polycrystalline $BiVO_4$, CR die solution can be completely removed. Furthermore, it is clearly seen that the degradation rate of the samples obtained in the presence of melamine is quite higher (90 % in 60 min) than that of the polycrystalline $BiVO_4$ sample (55 % in 60 min). It is quite obvious that melamine addition in experimental reaction system has a positive influence on the photocatalytic activity of the as-prepared porous $BiVO_4$ samples. Figure 9 shows the amount of absorbance of CR

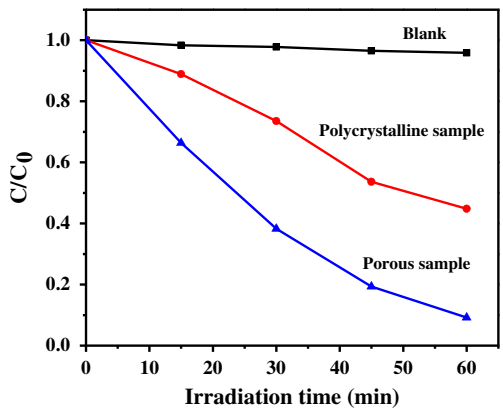

Fig. 8 Comparison of photocatalytic activities of as-prepared samples for the photocatalytic decolorization of CR aqueous solution

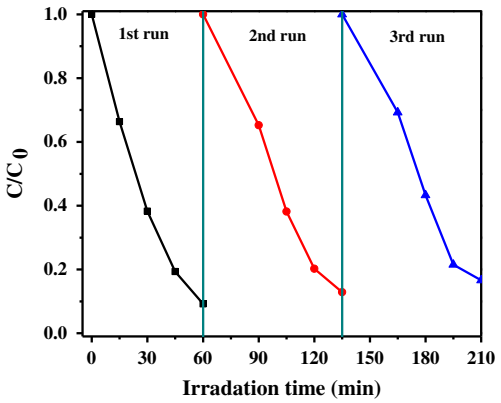

Fig. 10 Cycling runs in the photocatalytic degradation of CR in the presence of meso/macroporous $BiVO_4$ particles under visible light

aqueous solution as a function of time in the presence of as-prepared samples. This result clearly shows the important role played by melamine in the observed degradation of CR aqueous solution. The photocatalytic decolonization of CR aqueous solution follows a pseudo-first-order reaction. The determined apparent rate constant k for as-prepared porous $BiVO_4$ materials had the highest k value (0.04 min^{-1}) in the photodegradation of CR, while polycrystalline $BiVO_4$ particles (0.0140 min^{-1}) decreased compared with that of porous $BiVO_4$.

According to the above experimental results, the enhanced photocatalytic activity of hierarchical porous $BiVO_4$ materials can be attributed to the combined effect of several factors. Firstly, porous structures allow light scattering inside their pores, which enhances the light harvesting and thus increases the photogenerated electrons and holes to participate in the photocatalytic decomposition of the contaminants (Yu et al. 2010). Secondly, hierarchical porous structures could facilitate transportation of reactants and products on the photocatalyst surfaces and results in the easy chemical reaction (Zhang and Yu 2003; Wang et al. 2005). Last but not least, the large specific surface area and high crystallinity factors influence the photocatalytic activity of porous $BiVO_4$ sample.

In addition, further controlled experiments show that the porous $BiVO_4$ particles can be easily separated from the slurry system by filtration or sedimentation after photocatalytic reaction due to their high density and good mobility. Figure 10 shows the results of three successive CR aqueous dye solution degradation runs keeping other experimental conditions constant. It can be clearly seen that photocatalytic efficiency does not show major loss after three recycles and only a slight decrease in photodegradation efficiency is observed, indicating that the as-prepared porous $BiVO_4$ materials are relatively stable and do not photo-corrode during the reaction process.

Conclusion

In summary, meso/macroporous $BiVO_4$ materials with 400–600 nm in diameter were synthesized by a simple hydrothermal treatment, with the assistance of melamine as morphology-directing agent. The formation of the porous materials proceeds via a two-step process: first, the amorphous precursor gels were prepared, and then, in the presence of melamine, the gels were transformed into monoclinic $BiVO_4$ hierarchical bimodal porous materials. The as-prepared porous $BiVO_4$ material exhibits dense voids between and within porous particles which shows much higher photocatalytic activity than the polycrystalline materials for degradation of CR aqueous dye solutions under visible light irradiation, suggesting potential use for other future applications. In addition, this result may be extended to synthesis of other visible light-induced photocatalysts with suitable band gap and high activity for the environmental purification of organic pollutants in aqueous solution.

Acknowledgments The authors would like to thank Prof. B. Basavalingu and Prof. K. Byrappa, Department of Earth Science, University of Mysore, India for their valuable idea and discussions.

References

Amano F, Yamakata A, Nogami K, Osawa M, Ohtani B (2008) Visible light responsive pristine metal oxide photocatalyst: enhancement of activity by crystallization under hydrothermal treatment. J Am Chem Soc 130:17650–17651

Chen X, Zhang Z, Lee SW (2008) Selective solution/phase synthesis of BiOCl, $BiVO_4$ and δ-Bi_2O_3 nanocrystals in the reaction system of $BiCl_3$-NH_4VO_3-NaOH. J Solid State Chem 181:166–174

Galembeck A, Alves OL (2000) $BiVO_4$ thin film preparation by metalorganic decomposition. Thin Solid Films 365:90–93

Galembeck A, Alves OL (2002) Bismuth vanadate synthesis by metallo-organic decomposition: thermal decomposition study and particle size control. J Mater Sci 37:1923–1927

Gotić M, Musić S, Ivanda M, Šoufek M, Popović S (2005) Synthesis and characterization of bismuth (III) vanadate. J Mol Struct 744:535–540

Hazen RM, Mariathasan JWE (1982) Bismuth vanadate: a high-pressure, high-temperature crystallographic study of the ferroelectric-paraelastic transition. Science 216:991–993

Hirota K, Komatsu G, Yamashita M, Takemura H, Yamaguchi O (1992) Formation, characterization and sintering of alkoxy-derived bismuth vanadate. Mater Res Bull 27:823–830

Jiang HQ, Nagai M, Kobayashi K (2009) Enhanced photocatalytic activity for degradation of methylene blue over V_2O_5/$BiVO_4$ composite. J Alloys Compd 479:821–827

Kato H, Hori M, Konta R, Shimodaira Y, Kudo A (2004) Construction of Z-scheme type heterogeneous photocatalysis systems for water splitting into H_2 and O_2 under visible light irradiation. Chem Lett 33:1348–1349

Ke DN, Peng TY, Ma L, Cai P, Jiang P (2008) Photocatalytic water splitting for O_2 production under visible-light irradiation on $BiVO_4$ nanoparticles in different sacrificial reagent solutions. Appl Catal A 350:111–117

Ke DN, Peng TY, Ma L, Cai P, Dai K (2009) Effect of hydrothermal temperature on the microstructures of $BiVO_4$ and its photocatalytic O_2 evolution activity under visible light. Inorg Chem 48:4685–4691

Kohtani S, Koshiko M, Kudo A, Tokumura K, Ishigaki Y, Toriba A, Hayakawa K, Nakagaki R (2003) Photodegradation of 4-alkylphenols using $BiVO_4$ photocatalyst under irradiation with visible light from a solar simulator. Appl Catal B: Environ 46:573–586

Kudo A, Ueda K, Kato H, Mikami I (1998) Photocatalytic O_2 evolution under visible light irradiation on $BiVO_4$ in aqueous $AgNO_3$ solution. Catal Lett 53:229–230

Kudo A, Omori K, Kato H (1999) A novel aqueous process for preparation of crystal form-controlled and highly crystalline $BiVO_4$ powder from layered vanadates at room temperature and its photocatalytic and photophysical properties. J Am Chem Soc 121:11459–11467

Kudo A, Kato H, Tsuji I (2004) Strategies for the development of visible-light-driven photocatalysts for water splitting. Chem Lett 33:1534–1539

Li GS, Zhang DQ, Yu JC (2008) Ordered mesoporous $BiVO_4$ through nanocasting: a superior visible light-driven photocatalyst. Chem Mater 20:3983–3992

Lim AR, Lee KH, Choh SH (1992) Domain wall of ferroelastic $BiVO_4$ studied by transmission electron microscopy. Solid State Commun 83:185–186

Lim AR, Choh SH, Jang MS (1995) Prominent ferroelastic domain walls in $BiVO_4$ crystal. J Phys Condens Matter 7:7309–7323

Liu JB, Wang H, Wang S, Yan H (2003) Hydrothermal preparation of $BiVO_4$ powders. Mat Sci Eng B 104:36–39

Madhusudan P, Ran JG, Zhang J, Yu JG, Liu G (2011) Novel urea assisted hydrothermal synthesis of hierarchical $BiVO_4/Bi_2O_2CO_3$ nanocomposites with enhanced visible-light photocatalytic activity. Appl Catal B Environ 110:286–295

Mahapatra S, Giridhar M, Guru Row TN (2007) Structural and photocatalytic activity of lanthanide (Ce, Pr, and Nd) molybdovanadates. J Phys Chem C 111:6505–6511

Mahapatra S, Nayak SK, Giridhar M, Guru Row TN (2008) Microwave synthesis and photocatalytic activity of nano lanthanide (Ce, Pr, and Nd) orthovanadates. Ind Eng Chem Res 47:6509–6516

Patterson M, Shelden CE, Stockton BH (1977) Kubelka-Munk optical properties of a barium sulfate white reflectance standard. Appl Opt 16:729–732

Ren L, Jin L, Wang JB, Yang F, Qiu MQ, Yu Y (2009) Template-free synthesis of $BiVO_4$ nanostructures: I. Nanotubes with hexagonal cross sections by oriented attachment and their photocatalytic property for water splitting under visible light. Nanotechnology 20:115603

Shang M, Wang WZ, Zhou L, Sun SM, Yin WZ (2009) Nanosized BiVO4 with high visible-light-induced photocatalytic activity: ultrasonic-assisted synthesis and protective effect of surfactant. J Hazard Mater 172:338–344

Sing KSW, Everett DH, Haul RAW, Moscou L, Pierotti RA, Rouguerol J, Siemieniewska T (1985) Reporting physisorption data for gas/solid systems with special reference to the determination of surface area and porosity. Pure Appl Chem 57:603–619

Sleight AW, H-y C, Ferretti A, Cox DE (1979) Crystal growth and structure of $BiVO_4$. Mater Res Bull 14:1571–1581

Stoltzfus MW, Woodward PM, Seshadri R, Klepeis JH, Bursten B (2007) Structure and bonding in $SnWO_4$, $PbWO_4$, and $BiVO_4$: lone pairs vs inert pairs. Inorg Chem 46:3839–3850

Sun SM, Wang WZ, Zhou L, Xu H (2009) Efficient methylene blue removal over hydrothermally synthesized starlike $BiVO_4$. Ind Eng Chem Res 48:1735–1739

Tokunaga S, Kato H, Kudo A (2001) Selective preparation of monoclinic and tetragonal $BiVO_4$ with scheelite structure and their photocatalytic properties. Chem Mater 13:4624–4628

Wang XC, Yu JC, Ho CM, Hou Y, Fu XZ (2005) Photocatalytic activity of a hierarchically macro/mesoporous titania. Langmuir 21:2552–2559

Xu HY, Wang H, Yan H (2007) Preparation and photocatalytic properties of YVO_4 nanopowders. J Hazard Mater 144:82–85

Xu H, Li HM, Wu CD, Chu JY, Yan YS, Shu HM, Gu Z (2008) Preparation, characterization and phtocatalytic properties of Cu-loaded $BiVO_4$. J Hazard Mater 153:877–884

Xu YH, Liu CJ, Chen MJ, Liu YQ (2011) A review in visible-light-driven $BiVO_4$ photocatalysts. Int J Nanoparticles 4:268–283

Ye J, Zou ZG, Oshikiri M, Matsushita A, Shimoda M, Imai M, Shishido T (2002) A novel hydrogen-evolving photocatalyst $InVO_4$ active under visible light irradiation. Chem Phys Lett 356:221–226

Yin WZ, Wang WZ, Zhou L, Sun SM, Zhang L (2010) CTAB-assisted synthesis of monoclinic $BiVO_4$ photocatalyst and its highly efficient degradation of organic dye under visible-light irradiation. J Hazard Mater 173:194–199

Yu J, Kudo A (2006) Effects of structural variation on the photocatalytic performance of hydrothermally synthesized $BiVO_4$. Adv Funct Mater 16:2163–2169

Yu JG, Zhang J, Jaroniec M (2010) Preparation and enhanced visible-light photocatalytic H_2-production activity of CdS quantum dots-sensitized $Zn_{1-x}Cd_xS$ solid solution. Green Chem 12:1611–1614

Zhang L, Yu JC (2003) A sonochemical approach to hierarchical porous titania spheres with enhanced photocatalytic activity. Chem Commun 16:2078–2079

Zhang AP, Zhang JZ (2009) Characterization of visible-light-driven $BiVO_4$ photocatalysts synthesized via a surfactant-assisted hydrothermal method. Spectrochim Acta A 73:336–341

Zhang L, Fu H, Zhang C, Zhu Y (2006a) Synthesis, characterization, and photocatalytic properties of $InVO_4$ nanoparticles. J Solid State Chem 179:804–811

Zhang L, Chen DR, Jiao XL (2006b) Monoclinic structured $BiVO_4$ nanosheets: hydrothermal preparation, formation mechanism, and coloristic and photocatalytic properties. J Phys Chem B 110:2668–2673

Zhang X, Ai ZH, Jia FL, Zhang LZ, Fan XX, Zou ZG (2007) Selective synthesis and visible-light photocatalytic activities of $BiVO_4$ with different crystalline phases. Mater Chem Phys 103:162–167

Zhang HM, Liu JB, Wang H, Zhang WX, Yan H (2008) Rapid microwave-assisted synthesis of phase controlled $BiVO_4$ nanocrystals and research on photocatalytic properties under visible light irradiation. J Nanopart Res 10:767–774

Zhou L, Wang WZ, Zhang LS, Xu HL, Zhu W (2007) Single-crystalline $BiVO_4$ microtubes with square cross-sections: microstructure, growth mechanism, and photocatalytic property. J Phys Chem C 111:13659–13664

Zhou Y, Vuille K, Heel A, Probst B, Kontic R, Patzke GR (2010a) An inorganic hydrothermal route to photocatalytically active bismuth vanadate. Appl Catal A: General 140:140–148

Zhou B, Zhao X, Liu HJ, Qu JH, Huang CP (2010b) Visible-light sensitive cobalt-doped $BiVO_4$ (Co-$BiVO_4$) photocatalytic composites for the degradation of methylene blue dye in dilute aqueous solutions. Appl Catal B: Environ 99:214–221